Letters

An Arbitrary-Frequency Dual-Band High-Efficiency Rectifier Employing a Novel Frequency-Selective Power Allocation Network

Haoming He, *Graduate Student Member, IEEE*, Chongwei Liao, *Graduate Student Member, IEEE*, Zhongqi He, Liping Yan, *Senior Member, IEEE*, and Changjun Liu, *Senior Member, IEEE*

***Abstract*—This letter presents a novel frequency-selective power allocation network enabling high-efficiency arbitrary dual-band microwave rectification. The proposed design utilizes a frequency-selective network (FSN), composed of two pairs of quarter-wavelength transmission lines, which uniquely achieves power allocation by frequency-dependent impedance transformation, allowing independent optimization of each subrectifier. This approach significantly improves rectification efficiency at both frequencies and extends the optimal input power range. The FSN also reduces impedance variations, further enhancing the rectifier's performance. The proposed design method applies to rectifiers operating at arbitrary dual frequencies. A prototype dual-band rectifier operating at 2.45 and 5.8 GHz is designed, fabricated, and tested. The experimental results demonstrate peak efficiencies of 78.62% and 63.4% at 2.45 and 5.8 GHz, respectively. Moreover, the RF-dc power conversion efficiency exceeds 50% over a wide input power range (–2 to 18.3 dBm at 2.45 GHz and 3–19.7 dBm at 5.8 GHz), corresponding to input power dynamic ranges of 20.3 and 16.7 dB, respectively.**

***Index Terms*—Dual band, frequency selection, microwave rectifier, microwave wireless power transmission (WPT), wide input power range.**

I. Introduction

RAPID proliferation of Internet of Things (IoT) devices has fueled a growing demand for efficient and reliable wireless power transmission (WPT) technologies, eliminating the need for battery replacement and enabling truly autonomous operation [1], [2], [3], [4]. WPT offers a promising solution for powering wireless sensor networks, simplifying maintenance, and extending the lifetime of these devices [5], [6], [7], [8]. One approach to achieve stable and continuous powering of wireless sensor systems is through dual-band WPT [9], [10].

Received 9 January 2025; revised 12 February 2025; accepted 3 March 2025. Date of publication 5 March 2025; date of current version 14 April 2025. This work was supported in part by the National Natural Science Foundation of China under Grant U22A2015 and Grant 62401382 and in part by the Sichuan Science and Technology Program under Grant 2024YFHZ0282. *(Corresponding authors: Liping Yan; Changjun Liu.)*

The authors are with the College of Electronics and Information Engineering, Sichuan University, Chengdu 610064, China, and also with the Yibin Industrial Technology Research Institute of Sichuan University, Yibin 644000, China (e-mail: liping_yan@scu.edu.cn; cjliu@ieee.org).

Color versions of one or more figures in this article are available at https://doi.org/10.1109/TPEL.2025.3548282.

Digital Object Identifier 10.1109/TPEL.2025.3548282

However, achieving high RF-dc power conversion efficiency (PCE) across multiple frequency bands and a wide input power range presents a significant challenge, particularly due to the nonlinear behavior of rectifying diodes and the difficulty in achieving optimal impedance matching at multiple frequencies simultaneously [11], [12]. While previous research has explored dual-band rectifiers using various impedance matching techniques [13], [14], [15], these methods often involve complex design procedures and struggle to maintain high efficiency over wide power ranges, particularly at arbitrary frequency ratios. For instance, Liu et al. [15] achieved high efficiency at specific frequencies by relying on complex impedance transformations. Similarly, Hamano et al. [16] and Wang et al. [17] presented alternative approaches. They also face limitations in terms of design complexity, operating bandwidth, or power handling capability. The approach in [18] offers an interesting impedance compression method. Its applicability to arbitrary frequency ratios and wide power ranges remains unclear.

To address these challenges, this letter proposes a novel high-efficiency arbitrary dual-band rectifier design based on a frequency-selective network (FSN) that employs a unique power allocation technique. This FSN, composed of two pairs of quarter-wavelength microstrip transmission lines (TLs), effectively separates and directs input power at two distinct frequencies to dedicated subrectifiers, enabling independent optimization and simplified impedance matching. This approach not only simplifies the design process but also achieves high rectification efficiency across arbitrary dual frequencies. In addition, the FSN structure incorporates an impedance compression effect to mitigate changes in the rectifier impedance due to input power fluctuations, resulting in a wider input power range. The fabricated rectifier demonstrates a wide input power range and high efficiency.

II. Principle and Design Method

Fig. 1 depicts the schematic of the proposed arbitrary dual-band rectifier design. It utilizes an FSN consisting of two pairs of quarter-wavelength TLs and two subrectifiers operating at distinct frequencies, f_1 and f_2. Each subrectifier is designed to achieve high rectification efficiency at its corresponding frequency. By connecting the two rectifiers in parallel through the

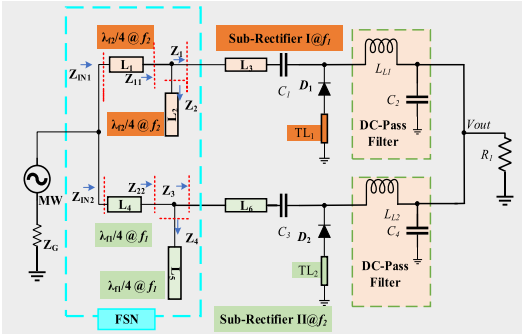

Fig. 1. Schematic of the proposed dual-band rectifier based on the FSN.

FSN, each rectifier can operate at its optimized frequency for maximum efficiency. This is achieved through a novel power allocation technique, where the FSN selectively directs the input power to the appropriate subrectifier based on its frequency. Simultaneously, the nonoperating subrectifier presents a high inductive impedance under the FSN impedance transformation, effectively compressing the input impedance of the other subrectifier. This contributes to widening the optimal input power range of the rectifier at both frequency bands.

A. Principle of the FSN

To illustrate the design principle, let us consider that the operating frequency of subrectifier I is f_1. The subrectifiers I and II are connected in parallel and the input impedance of rectifier I is $Z_{\mathrm{IN1}} = R_1 + jX_1$. To match the microwave source, Z_{IN1} is designed to be 50 Ω. To avoid any influence on subrectifier I at f_1, the input impedance $Z_{\mathrm{IN2}} = R_2 + jX_2$ of rectifier II needs to be as high as possible, much greater than 50 Ω. This ensures that subrectifier II has a negligible impact on subrectifier I. Assuming a source impedance of 50 Ω, and according to the principles of parallel circuits, the power distribution between subrectifiers I and II can be approximated as

$$\frac{P_1}{P_2} = \frac{\mathrm{Re}(Y_1)}{\mathrm{Re}(Y_2)} = \frac{\mathrm{Re}(1/Z_{\mathrm{IN1}})}{\mathrm{Re}(1/Z_{IN2})} = \frac{R_1(R_2^2 + X_2^2)}{R_2(R_1^2 + X_1^2)} \quad (1)$$

where P_1 and P_2 are the received power of rectifiers I and II, respectively, and Y_1 and Y_2 are the admittances of subrectifiers I and II, respectively. When $\mathrm{Re}(Y_1) >> \mathrm{Re}(Y_2)$, it can be approximated that all the incident power is received by rectifier I at f_1, and no power is accepted by rectifier II. This ensures high conversion efficiency at both frequency points of the rectifier.

At frequency f_1, when very little power passes through diode D_2 in subrectifier II, D_2 does not operate as the input voltage is lower than its turn-ON voltage. In this state, D_2 can be modeled as a capacitor with Z_3 representing its capacitive impedance. After impedance transformation through a quarter-wavelength TL, Z_{IN2} becomes equivalent to an inductive impedance, effectively presenting as a short-circuit microstrip line, as shown in Fig. 2 (which depicts the equivalent circuit at frequency f_1). As the input power fluctuates, Z_{IN1} changes significantly due to the nonlinearity of diode D_1. However, Z_{IN2} remains a relatively constant high inductive impedance ($Z_{\mathrm{IN2}} = jX_2$). The parallel

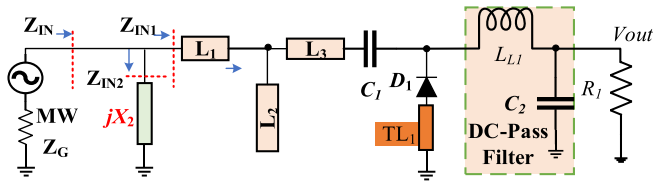

Fig. 2. Equivalent circuit of rectifier I at f_1 alone.

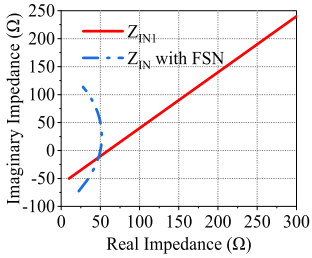

Fig. 3. Comparison of impedance compression effects with parallel connection of Z_{IN2}.

combining of these impedances, $Z_{\mathrm{IN}} = Z_{\mathrm{IN1}} \,//\, Z_{\mathrm{IN2}} = (R_1 + jX_1) \,//\, jX_2$, results in a more stable variation of Z_{IN}.

Fig. 3 demonstrates the impedance compression effect achieved by connecting Z_{IN2} in parallel. Z_{IN} exhibits impedance variation within a limited range when $Z_{\mathrm{IN2}} = j150$ Ω, while Z_{IN1} transforms from $(10 - j50)$ Ω to $(300 + j250)$ Ω. This clearly shows that Z_{IN} fluctuates less than Z_{IN1}, meaning that Z_{IN} can remain relatively stable despite impedance variations under different operating conditions. Therefore, the FSN effectively compresses the complex impedance, improving the system's stability and efficiency. This holds true regardless of whether the impedance changes are caused by the operating characteristics of nonlinear components or other factors.

Furthermore, when the input power is low, the input impedance is typically low and capacitive. The FSN effectively compensates for this input impedance, improving the matching effect of the rectifier at lower power levels, thus broadening the rectifier's high-efficiency range at low input power.

The isolation capacitor C_3 in subrectifier II serves as an open circuit to dc, ensuring that the output dc is not affected. This is essential because it prevents current from flowing back into the FSN when the diode is reverse biased, maintaining the intended power flow. This configuration allows the two subrectifiers to share the same dc load without negatively impacting each other's performance.

B. Design of the FSN

To prevent any energy from flowing into subrectifier II, it is necessary to increase the imaginary impedance of Z_{IN2}. As discussed in Section II-A and shown in (1), a more effective design approach is to increase the imaginary part of Z_{IN2} while decreasing its real part. The use of a quarter-wavelength TL in the FSN is an effective solution, as it allows the input impedance Z_{IN2} of rectifier II to approximate an open circuit. As illustrated in Fig. 1, an equivalent short-circuit point is achieved by the

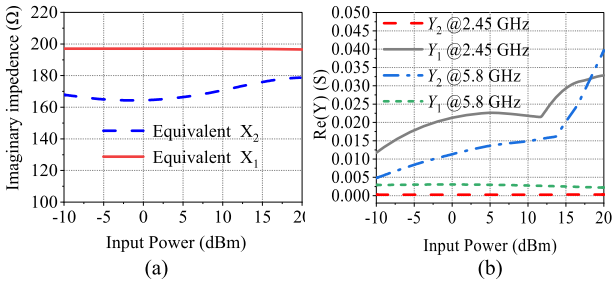

Fig. 4. (a) Equivalent inductive impedance of the optimized FSN at different frequencies. (b) Conductance variation curves of optimized FSN at different frequencies.

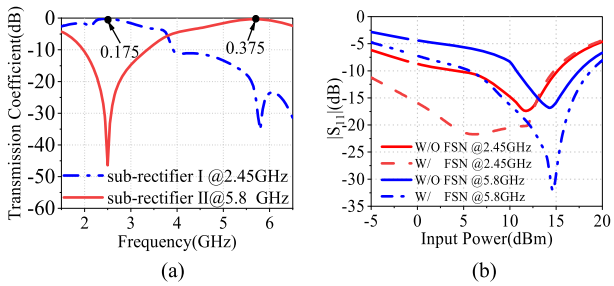

Fig. 5. (a) Voltage transmission coefficients of the FSN. (b) Comparison of $|S_{11}|$ of the rectifier, with and without the FSN, with the variation of input power at 2.45 and 5.8 GHz.

quarter-wavelength open ended at f_1 and $Z_4 = 0$. The impedance Z_{22}, which is in parallel with Z_3, is capacitive. In addition, the length of TL L_4 is also set to a quarter wavelength at f_1, ensuring that the imaginary part of the input impedance $\mathrm{Im}(Z_{\mathrm{IN2}})$ is approximately infinite, as expressed as follows:

$$Z_{\mathrm{IN2}} = Z_4 \frac{Z_{22} + jZ_4 \tan(\theta_4)}{Z_4 + jZ_{22} \tan(\theta_4)} = \frac{{Z_4}^2}{Z_{22}} \to \infty \tag{2}$$

where Z_4 and θ_4 are the characteristic impedance and electrical length of L_4. A high inductive impedance is obtained by adjusting the microstrip line lengths L_4 and L_5.

Meanwhile, the proposed FSN effectively compresses the variation in input impedance, thereby extending the input power dynamic range of the rectifier. There are no specific requirements for the characteristic impedance of each branch in the FSN, meaning that the width of each microstrip line can vary. This flexibility allows the width of the branch microstrip lines to serve as tuning variables, optimizing the equivalent inductance and matching the input impedance of rectifier II. Similarly, the tuning of microstrip lines L_1 and L_2 is carried out in the same manner.

To validate the theoretical framework and demonstrate the practical feasibility of the proposed design, FSNs operating at 2.45 and 5.8 GHz were designed and integrated with their respective high-efficiency subrectifiers. Comprehensive simulations were conducted using the Advanced Design System software, with f_1 and f_2 assigned to 2.45 and 5.8 GHz, respectively. The equivalent inductive impedance and the real part of the admittance of the optimized FSN, as functions of frequency, are depicted in Fig. 4(a) and (b), respectively. Fig. 4(a) and (b) illustrate the frequency-selective behavior of the FSN, demonstrating its ability to present a high inductive impedance at the nonoperating frequency. Further analysis of the RF input power distribution was performed based on these admittance parameters. As illustrated in Fig. 5(a), the simulated transmission coefficients $|S_{21}|$ of the FSN are -0.175 dB at 2.45 GHz and -0.375 dB at 5.8 GHz, indicating that 96% and 92% of the incident power are effectively delivered to the corresponding subrectifiers, respectively. This confirms the high efficiency of the power allocation mechanism.

Moreover, Fig. 5(b) presents a comparative analysis of the input reflection coefficient $|S_{11}|$ of the rectifier with and without the FSN at both operating frequencies. The results demonstrate a significant improvement in impedance matching when the FSN is incorporated, particularly evident in the reduction of $|S_{11}|$ across a wide input power range. This improvement is attributed to the impedance compression effect of the FSN, which effectively mitigates variations in the input impedance caused by fluctuations in input power. Consequently, the proposed FSN demonstrably extends the dynamic range of input power over which high efficiency is maintained.

In Fig. 1, TL_1 and TL_2 are $\lambda_g/8$ short-ended TLs at f_1 and f_2, respectively [19]. Its input impedance is given by

$$\begin{aligned} Z_{\mathrm{TL}i} &= jZ_{\mathrm{TL}i} \tan\left(\frac{\pi}{4}\frac{f}{f_0}\right) \\ &= \begin{cases} 0, & f = 0 \\ jZ_{\mathrm{TL}i}, & f = f_0 \\ \infty, & f = 2f_0 \\ -jZ_{\mathrm{TL}i}, & f = 3f_0 \end{cases}, \quad i = 1, 2 \end{aligned} \tag{3}$$

where $Z_{\mathrm{TL}1}$ and $Z_{\mathrm{TL}2}$ are the characteristic impedances of TL_1 and TL_2, respectively. It presents an inductive impedance at the operating frequency and can compensate for the capacitive of the diode impedance. Infinity impedance at $2f_0$ suppresses the second harmonic generated from rectifying to improve efficiency.

III. Implementation and Measurement

To experimentally validate the proposed design, a prototype dual-band rectifier operating at 2.45 and 5.8 GHz was fabricated. The layout, dimensions, and a photograph of the fabricated rectifier are presented in Fig. 6. The rectifier was realized on a 1-mm-thick F4B-2 substrate, a polytetrafluoroethylene (PTFE)-based microfiber glass composite material, possessing a relative dielectric constant of 2.65 and a loss tangent of 0.0012. The design incorporates two Avago HSMS286 Schottky barrier diodes. To mitigate the parasitic effects of inductance at the higher operating frequency, the 5.8-GHz subrectifier incorporates a dc-pass output filter comprising a quarter-wavelength microstrip line shunted by a capacitor.

The input reflection coefficient $|S_{11}|$ of the fabricated rectifier was measured using an Agilent N5230A vector network analyzer. A comparison between the measured and simulated $|S_{11}|$ at both operating frequencies is presented in Fig. 7(a).

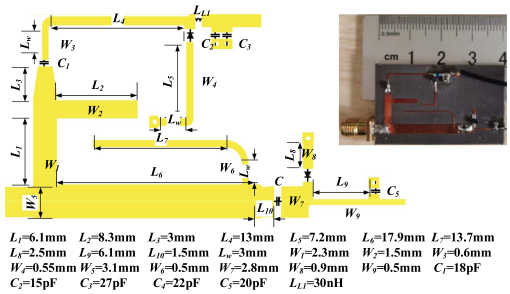

Fig. 6. Layout and photograph of the proposed dual-band rectifier.

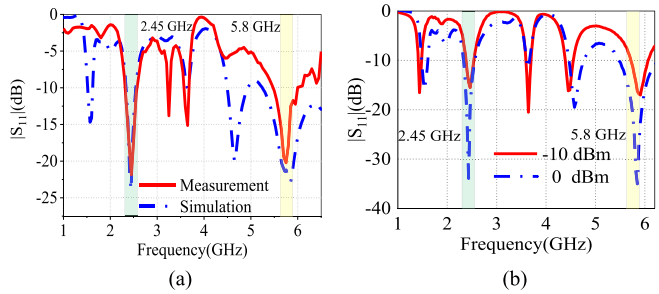

Fig. 7. (a) Simulated and measured $|S_{11}|$ at 11 dBm. (b) Measured $|S_{11}|$ at -10 and 0 dBm.

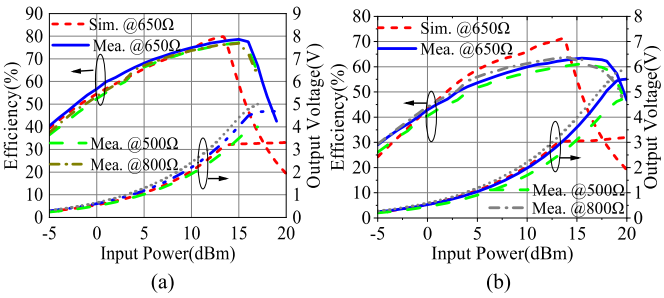

Fig. 8. Efficiency and output voltage of simulated and measured efficiency at (a) 2.45 GHz and (b) 5.8 GHz.

Excellent agreement between the measured and simulated results is observed, validating the accuracy of the design and simulation models. At an input power of 11 dBm, the measured $|S_{11}|$ remains below -20 dB at both frequencies, indicating a good impedance match. Furthermore, as illustrated in Fig. 7(b), the rectifier maintains a robust impedance match across a range of input power levels, highlighting the effectiveness of the FSN in achieving wide power range performance.

Fig. 8(a) presents the measured PCE of the rectifier with different dc loads as a function of input power at 2.45 GHz. A peak PCE of 78.62% is achieved at 15 dBm with a 650-Ω load. Notably, the rectifier maintains a PCE above 50% over a wide input power range from -2.0 to 18.3 dBm, corresponding to a dynamic range of 20.3 dB. Similarly, at 5.8 GHz, as depicted in Fig. 8(b), the rectifier exhibits a maximum PCE of 63.4% at an input power of 15.5 dBm and the same load, while maintaining a PCE above 50% for an input power range of 3.0–19.7 dBm, resulting in a dynamic range of 16.7 dB. It is worth noting that a slight frequency shift is observed between the measured and simulated PCE results. This shift can be attributed to minor variations introduced during the fabrication process and potential inaccuracies in the diode model.

TABLE I
COMPARISON WITH PREVIOUS RECTIFIERS

Ref	[12]	[15]	[17]	[18]	**This work**
Frequency (GHz)	2.45/5.8	0.915/ 2.45	2.38/ 4.99	2.45/ 5.8	**2.45 / 5.8**
Maximum efficiency	74.9%/ 61.9%	77.2% /73.5%	69.4% /55.3%	76.2%/ 61%	**78.6% /63.4%**
Input Power(dBm)	17	14.6	5	18.1/ 18.4	**15.0/ 15.5**
Power range (>50%,dB)	13.0/13.0	17.0/ 16.0	15.0/ 10.0	16.0/ 6.0	**20.3/ 16.7**
Size (mm^2)	49×42	60×33	N/A	N/A	**39×25**
Diode	HSMS 2860	HSMS 2862	BAT15 -03W	HSMS 286F	**HSMS 286F**
Diode number	1	2	2	4	**2**

Table I presents a comparative analysis of the proposed rectifier's performance against previously published works. The proposed rectifier demonstrates superior performance, achieving the highest measured efficiency and widest input power dynamic range.

IV. CONCLUSION

This letter presents a high-efficiency arbitrary dual-band rectifier that leverages a novel FSN to achieve both high efficiency and a wide input power dynamic range. The innovative FSN architecture facilitates automatic power allocation between subrectifiers optimized for specific frequencies while simultaneously mitigating input impedance variations induced by input power fluctuations. Experimental results agree with the efficacy of the proposed design, demonstrating peak efficiencies of 78.62% and 63.4% at 2.45 and 5.8 GHz, respectively. Furthermore, wide input power dynamic ranges of 20.3 and 16.7 dB were achieved at these respective frequencies. The proposed rectifier, due to its superior performance characteristics and compact form factor, holds significant promise for diverse applications, including wireless power transfer systems, energy harvesting for IoT devices, and power systems in the aerospace industry.

REFERENCES

[1] K. Danget et al., "A 5.8 GHz high-power and high-efficiency rectifier circuit with lateral GaN Schottky diode for wireless power transfer," *IEEE Trans. Power Electron.*, vol. 35, no. 3, pp. 2247–2252, Mar. 2020.

[2] Z. He, L. Yan, and C. Liu, "An adaptive Power Division strategy for nonlinear components in rectification," *IEEE Trans. Power Electron.*, vol. 39, no. 12, pp. 15436–15440, Dec. 2024.

[3] Y. Han, O. Leitermann, D. A. Jackson, J. M. Rivas, and D. J. Perreault, "Resistance compression networks for radio-frequency power conversion," *IEEE Trans. Power Electron*, vol. 22, no. 1, pp. 41–53, Jan. 2007.

[4] C. Liu, H. Lin, Z. He, and Z. Chen, "Compact patch rectennas without impedance matching network for wireless power transmission," *IEEE Trans. Microw. Theory Techn.*, vol. 70, no. 5, pp. 2882–2890, May 2022.

[5] C. Xu, Y. Zhuang, C. Song, Y. Huang, and J. Zhou, "Dynamic wireless power transfer system with an extensible charging area suitable for moving objects," *IEEE Trans. Microw. Theory Techn.*, vol. 69, no. 3, pp. 1896–1905, Mar. 2021.

[6] W. Zhong and S. Hui, "Reconfigurable wireless power transfer systems with high energy efficiency over wide load range," *IEEE Trans. Power Electron*, vol. 33, no. 7, pp. 6379–6390, Jul. 2018.

[7] P. Kamalinejad, C. Mahapatra, Z. Sheng, S. Mirabbasi, V. C. M. Leung, and Y. L. Guan, "Wireless energy harvesting for the Internet of Things," *IEEE Commun. Mag.*, vol. 53, no. 6, pp. 102–108, Jun. 2015.

[8] J. Zhou, P. Zhang, J. Han, L. Li, and Y. Huang, "Metamaterials and metasurfaces for wireless power transfer and energy harvesting," *Proc. IEEE*, vol. 110, no. 1, pp. 31–55, Jan. 2022.

[9] Y. Y. Hu, S. Sun, H. Wu, S. Yang, and J. Hu, "Integrated coupler-antenna design for multibeam dual-polarized patch-array rectenna," *IEEE Trans. Antennas Propag.*, vol. 70, no. 3, pp. 1869–1883, Mar. 2022.

[10] T. Ruan, Z. J. Chew, and M. Zhu, "Energy-aware approaches for energy harvesting powered wireless sensor nodes," *IEEE Sens. J.*, vol. 17, no. 7, pp. 2165–2173, Apr. 2017.

[11] H. Lin, X. Chen, Z. He, Y. Xiao, W. Che, and C. Liu, "Wide input power range X-band rectifier with dynamic capacitive self-compensation," *IEEE Microw. Wirel. Compon. Lett.*, vol. 31, no. 5, pp. 525–528, May 2021.

[12] S. Xiao, C. Liu, H. He, Y. Feng, and W. Che, "A novel class-F 2.45/5.8 GHz dual-band rectifier for wireless power transmission," *IEEE Microw. Wirel. Compon. Lett.*, vol. 34, no. 1, pp. 107–110, Jan. 2024.

[13] X. R. Dubey, S. K. Srivastava, A. Singh, and M. K. Meshram, "Compact and efficient dual-band rectifier using modified T-section matching network," *IEEE Microw. Wirel. Compon. Lett.*, vol. 33, no. 6, pp. 755–758, Jun. 2023.

[14] J. Liu, M. Huang, and Z. Du, "Design of compact dual-band RF rectifiers for wireless power transfer and energy harvesting," *IEEE Access*, vol. 8, pp. 184901–184908, 2020.

[15] J. Liu, Y. Z. Xiu, and C. L. Yang, "Analysis and design of dual-band rectifier using novel matching network," *IEEE Trans. Circuits Syst. II, Exp. Briefs*, vol. 65, no. 4, pp. 431–435, Apr. 2018.

[16] K. Hamano, A. Suzuki, K. Nishikawa, and S. Kawasaki, "2.4/5.8GHz dual-band rectifiers for aerospace wireless sensor and RF energy harvester system," in *Proc. IEEE Radio Wirel. Symp.*, May 2019, pp. 1–4.

[17] S. H. Wang, S. Y. Zheng, K. W. Leung, and M. H. Xia, "A self-matched multiband rectifier for efficient electromagnetic energy harvesting," *IEEE Trans. Circuits Syst. I, Reg. Papers*, vol. 68, no. 11, pp. 4556–4565, Nov. 2021.

[18] Z. X. Du and X. Y. Zhang, "High-efficiency single-and dual-band rectifiers using a complex impedance compression network for wireless power transfer," *IEEE Trans. Ind. Electron.*, vol. 65, no. 6, pp. 5012–5022, Jun. 2018.

[19] C. Liu, F. Tan, H. Zhang, and Q. He, "A novel single-diode microwave rectifier with a series band-stop structure," *IEEE Trans. Microw. Theory Techn.*, vol. 65, no. 2, pp. 600–606, Feb. 2017.